Distributed Computational Method for Coupled Fluid Structure Thermal Interaction Applications*

E. Aulisa[1], S. Manservisi[2], P. Seshaiyer[3,†], A. Idesman[4]
[1]Mathematics & Statistics, Texas Tech University, Lubbock, TX 79409, USA
[2]DIENCA-Lab. di Montecuccolino, Via dei Colli 16, 40136 Bologna, Italy
[3]Mathematical Sciences, George Mason University, Fairfax, VA 22030, USA
[4]Mechanical Engineering, Texas Tech University, Lubbock, TX 79409-1021, USA

Received 21/11/2008; Accepted 10/11/2009

ABSTRACT

The problem of effcient modeling and computation of the nonlinear interaction of fluid with a solid undergoing nonlinear deformation has remained a challenging problem in computational science and engineering. Direct numerical simulation of the non-linear equations, governing even the most simplified fluid-structure interaction model depends on the convergence of iterative solvers which in turn relies heavily on the properties of the coupled system. The purpose of this paper is to introduce a distributed multilevel algorithm with finite elements that offers the flexibility and efficiency to study coupled problems involving fluid-structure interaction. Our numerical results suggest that the proposed computational methodology for solving coupled problems involving fluid-structure interaction is reliable and robust.

1. INTRODUCTION

Distributed computing has evolved rapidly in the last decade. This has helped develop new computational methodologies to solve complex multi-physics

*This work is supported in part by the Computational Mathematics program, National Science Foundation under Grant DMS 0813825.
†Corresponding Author; email: pseshaiy@gmu.edu

problems involving fluidstructure interactions (FSI) efficiently. The efficient solution of such a coupled system provides predictive capability in studying complex nonlinear interactions that arise in several applications such as blood flow interaction with arterial wall [1, 2] to computational aeroelasticity of flexible wing micro-air vehicles [3], where the structural deformation and the flow field interact in a highly non-linear fashion. The direct numerical simulation of this highly non-linear system, governing even the most simplified FSI, depends on the convergence of iterative solvers which in turn relies on the characteristics of the coupled system.

Domain decomposition techniques with non-matching grids have become increasingly popular in this regard for obtaining fast and accurate solutions of problems involving coupled processes. The mortar finite element method [4, 5] has been considered to be a viable domain decomposition technique that allows coupling of different subdomains with nonmatching grids and different discretization techniques. The method has been shown to be stable mathematically and has been successfully applied to a variety of engineering applications [6, 7, 8]. The basic idea is to replace the strong continuity condition for matching grids at the interfaces between the different subdomains by a weaker one for problems involving non-matching grids to solve the problem in a coupled fashion. In the last few years, mortar finite element methods have also been developed in conjunction with multigrid techniques [9, 10, 11, 12, 13]. One of the great advantages of the multigrid approach is in the grid generation process wherein the corresponding refinements are already available and no new mesh structures are required. Also, the multigrid method relies only on local relaxation over elements and the solution on different domains can be easily implemented over parallel architectures.

The purpose of this paper is to introduce a distributed multigrid algorithm that can be used to study different physical processes over different subdomains involving non-matching grids with less computational effort. In particular, we develop the method for a problem that involves an Fluid-Structure-Thermal Interaction (FSTI). In section 2, the coupled model and governing equations are described together with their weak formulation. In section 3 the multigrid domain decomposition algorithm and a finite element discretization is discussed. Section 4 outlines the distributed computational methodology. Finally in section 5, we present the numerical experiments for the benchmark application described and follow that with discussion and conclusion in section 6.

2. MODEL AND GOVERNING EQUATIONS

In this section, we present a model for the interaction of a nonlinear structural domain interacting with a fluid medium. Note that for simplicity of presentation, we consider a model with a structural element to be a nonlinear beam and the methodology presented herein, can be extended to more complicated structural elements as well. Moreover, the methodology is described for a two-dimensional problem and can be extended to higher dimensions also. Let the rectangular region $\Omega = [4m] \times [2m]$ be the computational domain with boundary Γ (Figure 1).

Let Ω_f and Ω_s be the fluid and the solid subdomains, respectively. The solid region Ω_s consists of a beam, clamped at the point $(1m, 0)$, with length equal to $0.5\ m$ and thickness equal to $0.04\ m$. The fluid and the solid boundaries, Γ_f and Γ_s are the contours of the two shaded regions and their intersection is labeled by Γ_{sf}. Let $\Gamma_f^e = \Gamma \cap \Gamma_f$ and and $\Gamma_s^e = \Gamma \cap \Gamma_s$ be the fluid exterior boundary and the solid exterior boundary, respectively. For simplicity let us assume that the only boundary which can change in time is the interior boundary Γ_{sf}.

The unsteady Navier-Stokes equations for incompressible flows are considered in the fluid domain Ω_f, while the energy equation is solved in the whole domain Ω. In the solid region Ω_s the nonlinear Euler-Bernoulli beam equation is considered. In this approximation plane cross sections perpendicular to the axis of the beam are assumed to remain plane and perpendicular to the axis after deformation [14] and under these hypotheses only a one-dimensional model is required for describing the axial and transverse deflections of the

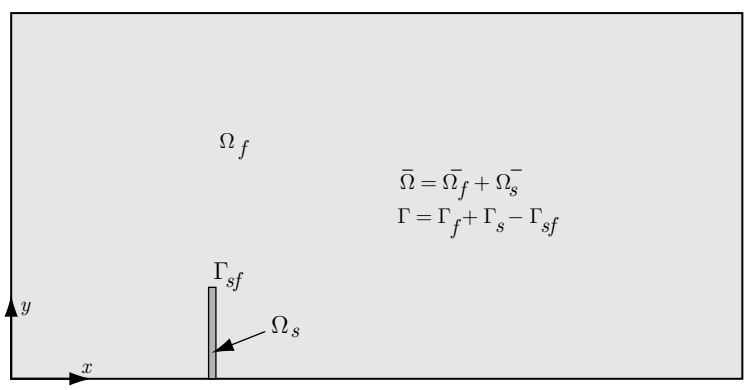

Figure 1. Computational domain for the FSTI problem.

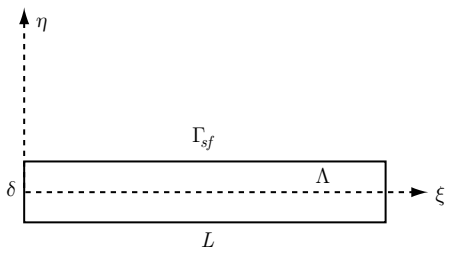

Figure 2. Nonlinear beam computational domain.

beam. We will denote by Λ the beam axis and by (ξ, η) a local reference system oriented with the ξ-axis parallel to Λ. As shown in Figure 2, variables δ and L are the thickness and the length of the beam respectively, the interior boundary Γ_{sf} is in $(\xi, \pm\, \delta/2)$ for $0 \le \xi \le L$ and in (L, η) for $-\delta/2 \le \eta \le \delta/2$.

Let $\Gamma_1 \subset \Gamma_f^e$ be the part of the boundary where Dirichlet boundary conditions are imposed for the velocity field $\vec{u} = (u_1,\ u_2)$; Neumann homogenous boundary conditions are considered on the remaining part, $\Gamma_f^e \backslash \Gamma_1$. Similarly, let $\Gamma_2 \subset \Gamma$ be the part of the boundary where Dirichlet boundary conditions are imposed for the temperature T, while Neumann homogenous boundary conditions are considered on $\Gamma \backslash \Gamma_2$. In $\xi = 0$ Dirichlet zero boundary conditions are imposed for the solid displacements and its appropriate derivatives. Conditions of displacement compatibility and force equilibrium along the structure-fluid interface Γ_{sf} are satisfied.

Let $\vec{U} \in \mathbf{H}^{1/2}(\Gamma_1)$ be the prescribed boundary velocity over Γ_1, satisfying the compatibility condition, and $\Theta \in H^{1/2}(\Gamma_2)$ be the prescribed temperature over Γ_2. Note that we use the standard Sobolev space [1] notation. The velocity, the pressure, the temperature and the beam deflections $(\vec{u}\,,\ p,\ T,\ w,\ d) \in \mathbf{H}^1(\Omega_f)$ $\times\ L^2(\Omega_f) \times H^1(\Omega) \times H^2(\Lambda) \times H^1(\Lambda)$ satisfy the weak variational form of the unsteady fully coupled system given by the Navier-Stokes system over Ω_f

$$< \rho_f \frac{\partial \vec{u}}{\partial t}, \vec{v}_f > + a_f(\vec{u}, \vec{v}_f) + b_f(\vec{v}_f, p) + c_f(\vec{u}; \vec{u}, \vec{v}_f) = - < \rho_f \vec{g} \beta (T - T_0), \vec{v}_f > \quad (1)$$

[1] We are using $H^k(\Omega)$ to denote the space of functions with k generalized derivatives. We set $L^2(\Omega) = H^0(\Omega)$ and note that the derivation of these spaces can be extended to non-integer values k by interpolation.

$$b_f(\vec{u}, r_f) = 0 \tag{2}$$

$$< \vec{u} - \vec{U}, \vec{s}_f > \Gamma_1 = 0 \tag{3}$$

$$< u_1 - \dot{w}, s_{sf} > \Gamma_{sf} = 0 \tag{4}$$

$$< u_2 - \dot{d}, s_{sf} > \Gamma_{sf} = 0 \tag{5}$$

the energy equation over Ω

$$< \rho\ c_p \frac{\partial T}{\partial t}, v > + a(T, v) + c(\vec{u}; T, v) = 0 \tag{6}$$

$$< T - \Theta, s > \Gamma_2 = 0 \tag{7}$$

and the nonlinear Euler-Bernoulli beam equation over Ω_s

$$\begin{aligned} &< \rho_s \delta \ddot{w}, v_s > + \ a_s(w, v_s) + c_s(d; w, v_s) = \\ &< p\left(\vec{x}\left(\xi, -\frac{\delta}{2}\right), t\right) - p\left(\vec{x}\left(\xi, \frac{\delta}{2}\right), t\right), v_s > \end{aligned} \tag{8}$$

$$< d_\xi + \frac{w_\xi^2}{2}, v_\xi > = 0 \tag{9}$$

$$w(0,t) = 0, \ \ \frac{\partial w(0,t)}{\partial \xi} = 0, \ \ \dot{w}(0,t) = 0, \ \text{ and } \ \ d(0,t) = 0 \tag{10}$$

describing the transverse deflection $w(\xi, t)$ and the axial beam deflection $d(\xi, t)$.

In eqns (1–2) the continuous bilinear and trilinear forms are defined as

$$a_f(\vec{u}, \vec{v}) = \int_{\Omega_f} 2\mu_f D(\vec{u}) : D(\vec{v}) d\vec{x} \tag{11}$$

$$b_f(\vec{v}, r) = -\int_{\Omega_f} r \nabla \cdot \vec{v} d\vec{x} \tag{12}$$

$$c_f(\vec{w};\vec{u},\vec{v}) = \int_{\Omega_f} \rho_f(\vec{w}\cdot\nabla)\vec{u}\cdot\vec{v}\,d\vec{x} \tag{13}$$

where ρ_f and μ_f are the density and the viscosity of the fluid. The distributed force in eqn (1) is the Boussinesq approximation of the buoyancy force, where $\vec{g}$ is the acceleration due to gravity, β the volumetric expansion coefficient of the fluid and T_0 a reference temperature. For $T > T_0$ the fluid expands then the density decreases and the buoyancy force points in the direction opposite to the gravity. When $T > T_0$ both the buoyancy force and the gravity point in the same direction. In eqn (6) the bilinear and trilinear forms are defined as

$$a(T,v) = \int_{\Omega} k\nabla T\cdot\nabla v\,d\vec{x} \tag{14}$$

$$c(\vec{u};T,v) = \int_{\Omega} \rho\, c_p(\vec{u}\cdot\nabla T)v\,d\vec{x} \tag{15}$$

where ρ, c_p, and k are the density, the heat capacity and the heat conductivity, respectively. If the integral is over the subdomain Ω_f , the fluid physical properties ρ_f, c_{pf}, and k_f are used, otherwise over Ω_s the solid properties ρ_s, c_{ps}, and k_s are used. Furthermore in the solid region the trilinear form $c(\vec{u}\,;\,T,\,v)$ is identically zero, since the velocity $\vec{u}$ is zero. In eqn (8) the bilinear form and the nonlinear term are given by:

$$a_s(w,v) = \int_{\Lambda} EI\ \ w_{\xi\xi}v_{\xi\xi}d\xi \tag{16}$$

$$c_s(d;w,v) = \int_{\Lambda} E\delta\left(d_{\xi} + \frac{1}{2}w_{\xi}^2\right)w_{\xi}v_{\xi}d\xi \tag{17}$$

where E is the Young's modulus and I the moment of inertia for unitary deepness. In the right hand side of eqn (8) the load due to the pressure difference between the two sides of the beam is given. Eqn (8) represents the force equilibrium constraint between the two subdomains Ω_f and Ω_s on the common boundary Γ_{sf} . For details concerning the function spaces, the bilinear and the trilinear forms and their properties, one may consult [15, 16]. Eqn (3), eqn (7) and eqn (10) represent the exterior Dirichlet boundary condition for the velocity, the temperature and the displacement, respectively. Eqns (4–5) represent the compatibility constraints between the velocity field $\vec{u}$ and the time derivative of the respective beam deflections on Γ_{sf}.

3. DOMAIN DECOMPOSITION & FINITE ELEMENT DISCRETIZATION

Let the domain Ω be partitioned into m non-overlapping sub-domains $\{\Omega^i\}_{i=1}^m$ such that $\partial\Omega^i \cap \partial\Omega^j \, (i \neq j)$ is either empty, a vertex, or a collection of edges of Ω^i and Ω^j. In the latter case, we denote this interface by Γ^{ij} which consists of individual common edges from the domains Ω^i and Ω^j. Let now the fluid domain Ω_f be partitioned into m non-overlapping sub-domains $\{\Omega_f^i\}_{i=1}^m$, where Ω_f^i is given by $\Omega_i \cap \Omega_f$. The fluid partition $\{\Omega_f^i\}_{i=1}^m$ is obtained from the domain partition $\{\Omega^i\}_{i=1}^m$, subtracting the solid region from each subdomain Ω^i, then Ω_f^i is an empty region if Ω^i is a subset of Ω_s. The common boundary between two subregions Ω_f^i and Ω_f^j is denoted by Γ_f^{ij}. The velocity, the pressure, the stress vector, the temperature, the heat flux and the displacements $(\vec{u}^i,\ p^i,\ \vec{\tau}^{ij},\ T^i,\ q^{ij},\ w,\ d)$ satisfy the following system of equations

$$< \rho_f \frac{\partial \vec{u}^i}{\partial t}, \vec{v}_f^i > + \ a_f(\vec{u}^i, \vec{v}_f^i) + \ b_f(\vec{v}_f^i, p^i) + \ c_f(\vec{u}^i; \vec{u}^i, \vec{v}_f^i) + < \vec{\tau}^{ij}, \vec{v}_f^i > \Gamma_f^{ij} \ = - < \rho_f \vec{g} \beta (T^i - T_0), \vec{v}_f^i > \tag{18}$$

$$b_f(\vec{u}^i,\, r_f^i) = 0 \tag{19}$$

$$< \vec{u}^i - \vec{U},\ \vec{s}_f^i > \Gamma_1^i \ = 0 \tag{20}$$

$$< \vec{u}^i - \vec{u}^j,\ \vec{s}_f^{ij} > \Gamma_f^{ij} \ = 0 \tag{21}$$

$$< u_1^i - \dot{w},\ s_{sf}^i > \Gamma_{sf}^i = 0 \tag{22}$$

$$< u_2^i - \dot{d},\ s_{sf}^i > \Gamma_{sf}^i = 0 \tag{23}$$

$$< \rho \ c_p \frac{\partial T^i}{\partial t}, v^i > + \ a(T^i, v^i) + \ c(\vec{u}^i; T^i, v^i) + < \vec{q}^{ij}, \vec{v}^i > \Gamma^{ij} = 0 \tag{24}$$

$$< T^i - \Theta, s^i > \Gamma_2^i = 0 \tag{25}$$

$$< T^i - T^j, \vec{s}^{ij} > \Gamma^{ij} = 0 \tag{26}$$

coupled with the beam eqns (8–10) for $i = 1, 2, \ldots, m$ where $\Gamma_1^i = \Gamma_1 \cap \partial\Omega_f^i$ and $\Gamma_2^i = \Gamma_2 \cap \partial\Omega^i$. The stress vector and heat flux are

$$\vec{\tau}^{ij} = -\mu \nabla \vec{u}^i \cdot \hat{n}_f^{ij} + p^i \hat{n}_f^{ij} \tag{27}$$

$$q^{ij} = -k \nabla T^i \cdot \hat{n}^{ij} \tag{28}$$

with $n_f^{ij}$and n^{ij} the unitary external vectors normal to the subdomains Ω_f^i and Ω^i, respectively.

Remark 1: In order to account for the changing nature of the fluid and solid subdomains, one must define a dynamic mesh for the space discretization. However, to avoid extreme distortion, we choose to move the mesh independently of the fluid velocity in the interior of Ω_f. Such a scheme, called arbitrary Lagrangian-Eulerian (ALE) formulation, is commonly applied when studying fluid-structure interaction [17, 18, 19, 20]. To account for this we introduce a grid velocity $\vec{u}_g$ which can be any velocity satisfying the constraints that it vanishes on Γ, it matches the fluid velocity on the interface Γ_{sf} and it is equal to the time derivative of the displacement in the solid domain. One can then express the Eulerian derivative as the difference between the Lagrangian derivative and the corresponding grid velocity advection term as follows:

$$\frac{\partial \vec{u}}{\partial t} = \frac{D\vec{u}(\vec{x}(t), t)}{Dt} - (\vec{u}_g \cdot \nabla)\vec{u}. \tag{29}$$

Substituting the new expression then into eqn (18) modifies the trilinear form to become $c_f(\vec{u}^i - \vec{u}_g^i; \vec{u}^i, \vec{v}_f^i)$. In a similar fashion the Eulerian derivative of the temperature is also expressed as a difference which modifies the corresponding trilinear form in eqn (24) to $c(\vec{u}^i - \vec{u}_g^i; T^i, v^i)$.

Remark 2: The structural equation is discretized in time by a using Newmark integration scheme. In this method the displacement and its time derivative are approximated according to:

$$w_{t+1} = w_t + \Delta t \dot{w}_t + 0.5 \Delta t^2 \, \ddot{w}_{t+\gamma} \tag{30}$$

$$\dot{w}_{t+1} = \dot{w}_t + \Delta t\, \ddot{w}_{t+\alpha} \tag{31}$$

$$\ddot{w}_{t+\theta} = (1-\theta)\ddot{w}_t + \theta\, \ddot{w}_{t+1} \tag{32}$$

In particular, the constant-average acceleration method $(\alpha = \gamma = 0.5)$ was employed which is known to be stable for each time step and conserves energy for free vibration problem [14].

Let us introduce a finite element discretization in each subdomain Ω^i through the mesh parameter h which tends to zero. Let $\{\Omega_h^i\}_{i=1}^m$ be the partition of the discretized domain Ω_h. Now, by starting at the multigrid coarse level $l = 0$, we subdivide each Ω_h^i and consequently Ω_h into triangles or rectangles by families of meshes $\mathcal{T}_h^{i,0}$. A typical refinement is illustrated in Figure 3.

Based on a simple element midpoint refinement different multigrid levels can be built to reach the finite element meshes $\mathcal{T}_h^{i,n}$ at the top finest multigrid

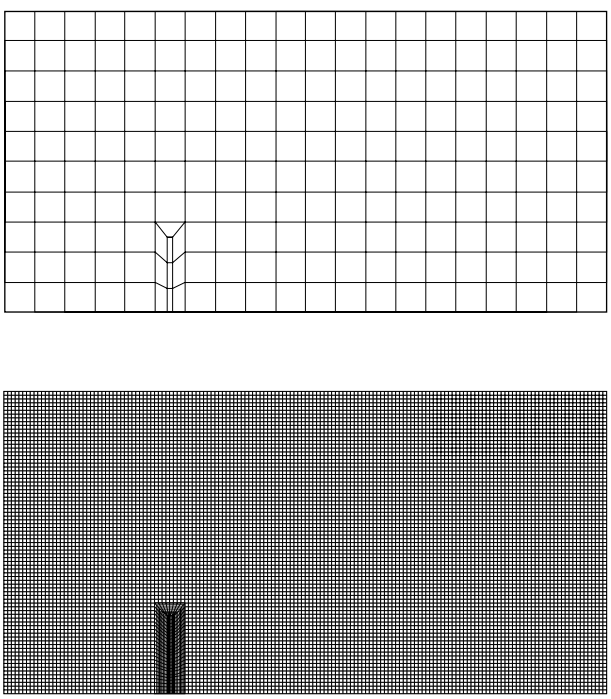

Figure 3. Coarse mesh l_0 (top) and fine mesh l_3 (bottom), built with three consecutive midpoint refinements.

level l_n. At the coarse level, as at the generic multigrid level l, the triangulation over two adjacent subdomains, Ω_h^i and Ω_h^j, obeys the finite element compatibility constraints along the common interfaces Γ_h^{ij} . For details on multigrid levels and their construction one may consult [21, 22]. By using this methodology we construct a sequence of meshes for each multigrid level in a standard finite element fashion with compatibility enforced across all the element interfaces built over midpoint refinements. In every subdomain Ω_h^i the energy equations can be solved over a different level mesh, generating a global solution over Ω_h, consisting mesh solutions at different levels over different subdomains. Let $\Omega_h^{i,l}$ be the subdomain i where the solution will be computed at the multigrid level l. It should be noted that the multigrid levels at which the solution is computed over adjacent subdomains, $\Omega_h^{i,l}$ and $\Omega_h^{j,k}$, may be different from each other $(l \neq k)$, with no compatibility enforced across the common interface Γ_h^{ij}.

4. DISTRIBUTED COMPUTATIONAL ALGORITHM

The solution to the associated fluid-structure-thermal interaction problem is then achieved via an iterative strategy, where four systems of equations are solved separately and in succession, always using the latest information, until convergence is reached. An iterative multigrid solver in conjuction with a Vanka type smoother [23] is used for the Navier-Stokes, the energy equation and the grid velocity equation systems. For the solution of the non-linear beam equation a direct nonlinear solver is used. The distributed computational algorithm employed is summarized in Figure 4.

At each iteration, the linearized Navier-Stokes system is assembled, using the latest updated value of the temperature T and the latest updated value of the grid velocity $\vec{u}_g$ in the nonlinear term $c_f(\vec{u}-\vec{u}_g;\vec{u},\vec{v}_f)$. In the nonlinear term, the first of the two velocity $\vec{u}$ is considered explicitly. On the boundary Γ_{sf} Dirichlet boundary conditions are imposed according to the latest updated value of the beam displacement time derivatives $\dot{w}$ and $\dot{d}$. A V-cycle multigrid algorithm is used to obtain a new updated solution for the pressure p and the velocity $\vec{u}$. Then the energy equation system is assembled, using the previously evaluated velocity and grid velocity in the advection term $c(\vec{u}-\vec{u}_g;T,v)$. A multigrid V-cycle is solved and updated values of the temperature T are found. Finally the beam equation system is built, where the load field is computed using the previous evaluated pressure p. Since the number of the subdomain unknowns is limited a direct nonlinear solver can be used for

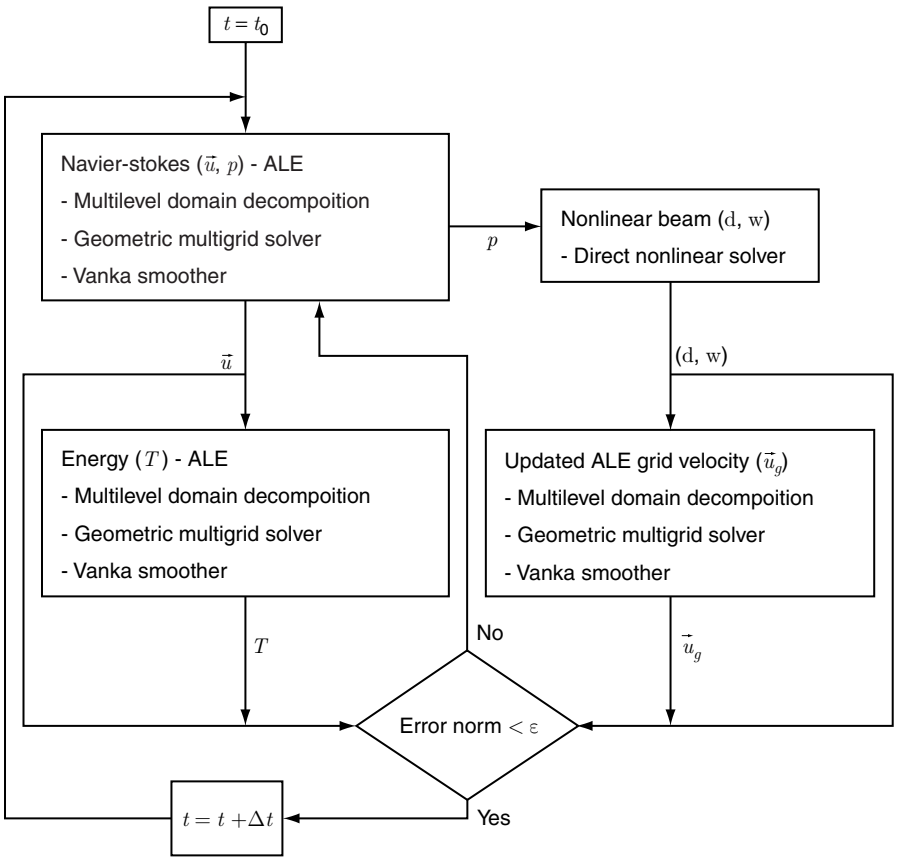

Figure 4. Distributed computational methodology for the FSTI problem.

computing the new displacements w and d and the appropriate time derivatives. The grid velocity is then computed to accomodate ALE and the grid nodes are advected along the corresponding characteristic lines. The whole procedure is repeated until convergence is finally reached.

The Navier-Stokes, energy and grid-velocity systems are solved using a fully coupled iterative multigrid solver [23] with a Vanka type smoother. Multigrid solvers for coupled velocity/pressure system compute simultaneously the solution for both the pressure and the velocity field, and they are known to be one of the best class of solvers for laminar Navier-Stokes equations (see for examples [21, 22]). The Vanka smoother employed in our multigrid solver involves the solution of a small number of degrees of freedom given by the conforming Taylor-Hood finite element discretization used. For this kind of

element the pressure is computed only at the vertices while the velocity field is computed also at the midpoints. Examples of computations with this kind of solver can be found in [9, 10, 11, 21, 22].

In order to increase the convergence rate, the considered Vanka type smoother has been coupled with a standard V-cycle multigrid algorithm. The multigrid does not change the nature of the solver, but allows the information to travel faster among different parts of the domain. A rough global solution is evaluated on the coarsest mesh $l = 0$ and projected on the finer grid $l = 1$, where Vanka-loops are performed improving the smaller aspects of the solution. The updated solution is then projected on the mesh level $l = 2$ and improved. The procedure is repeated until the finest mesh is reached. Solving the equation system in fine meshes improves solution details, but at the same time reduces the communication speed over the domain. However, this does not affect the global convergence rate since a considerable information exchange among different parts of the domain has been already done when solving in coarser mesh levels. All these considerations can be directly extended to the energy equation solver, where the same element block is considered.

5. NUMERICAL TESTS

In this section we test the performance of the distributed multilevel formulation for the FSTI application on the geometry described in Figure 1. On the left side of the domain inflow boundary conditions are imposed for the velocity field $\vec{u} = (u_1,\ u_2)$, with parabolic profile $u_1 = 0.1\ y\ (2-y)\ m/s$ and $u_2 = 0$. On the right side of the domain pressure outflow boundary conditions are imposed while on the remaining part of the boundary non-slip conditions are considered. The temperature is set equal to $0°\,C$ in the inlet region and to $100°\,C$ on the solid boundary where the beam is clamped. Adiabatic conditions are imposed on the rest of the domain. The initial conditions for both the temperature and the velocity field are zero.

The fluid and the solid properties are chosen in order to produce a large deformation of the beam. This choice may violate the assumption that cross sections perpendicular to the axis of the beam are assumed to remain plane and perpendicular to the axis after deformation. However it implies strong interactions among all the parts of the system and test the reliability and robustness of the solver in complex situations.

In the Navier-Stokes system, the fluid density, the viscosity, the volumetric expansion coefficient and the reference temperature are equal to $\rho_f = 100\ kg/m^3$, $\mu_f = 0.01\ Kg/ms$, $\beta = 0.01\ K^{-1}$ and $T_0 = 0°\,C$, respectively. In the energy

equation the solid density is $\rho_s = 200\ kg/m^3$. The heat capacity and the heat conductivity are $c_p = 100\ J/Kg\ K$ and $K = 10\ W/m\ K$, in the fluid region, and $c_p = 10\ J/Kg\ K$ and $K = 400\ W/m\ K$, in the solid region. The stiffness for unitary length of the beam is equal to $1\ kg\ m^2/s^2$.

In all the simulations the same time step $\Delta t = 0.01\ s$ is used, for a total of 500 time steps (5 seconds). Only the four mesh level configurations, l_0, l_1, l_2 and l_3, are considered and in Figure 3, the two different mesh configurations, l_0 and l_3, are shown. The coarse mesh l_0 has 207 elements, while the fine mesh l_3 obtained after three consecutive midpoint refinements has 13248 elements. The one-dimensional mesh on the beam axis follows the same midpoint refinement algorithm used for the two-dimensional computational domain Ω. On the coarse mesh level l_0 three elements are available, while on the fine grid l_3 after 3 refinements, the number of elements becomes 24. Since the number of unknowns is quite small, $(24 + 1) \times 2 = 50$, the solution of the non-linear beam equation is always evaluated on the finest mesh using a direct non-linear solver.

We apply the method to the following three types of model problems:

Case A	Coupled model with rigid beam
Case B	Coupled model with linear beam
Case C	Coupled model with nonlinear beam

The results obtained with our coupled model (case C) are compared with the results obtained for the same geometry with a rigid beam, $E = \infty$, and zero buoyancy force $\beta = 0$ (case A), and with the results obtained neglecting only the effects of the non-linear term (17) in the beam eqn (8) (case B). All the computations are done at the time $t = 5\ s$ and over the finest mesh level l_3.

In Figure 5 on the left, the beam bending and the corresponding grid deformation are displayed, showing the strong influence of the pressure load

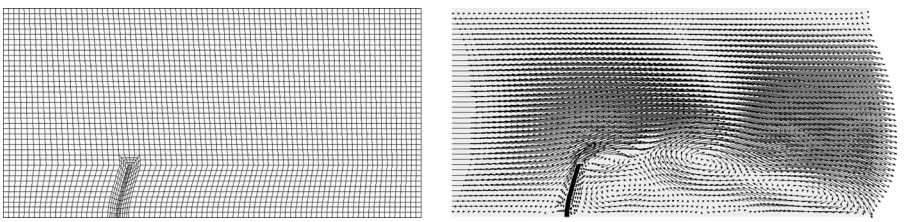

Figure 5. Beam bending and grid movement (left); Velocity Field Map (right).

on the beam shape. Figure 5 on the right shows the velocity field map and clearly indicates that the steady solution is not reached since new vortices are constantly created and advected towards the outflow region. In Figure 6 the velocity field (top), the pressure (bottom-left) and the temperature (bottom right) profiles, evaluated over the section $y = 0.5$ for $0 \leq x \leq 4$, are shown for all the three cases. The combined effect of the beam deflection and of the buoyancy force (case B and C) modify considerably all the profiles obtained in case A ($E = \infty$, and zero buoyancy force $\beta = 0$). Even the differences between case B and C are not negligible. The presence of the nonlinear term in the beam equation has considerable effects on all the solution profiles, pointing out how sensitive nature of the interaction among all the parts of the coupled system.

The number of unknowns (velocity field, pressure, temperature and displacement), involved in the computation at the mesh l_3 is approximatively

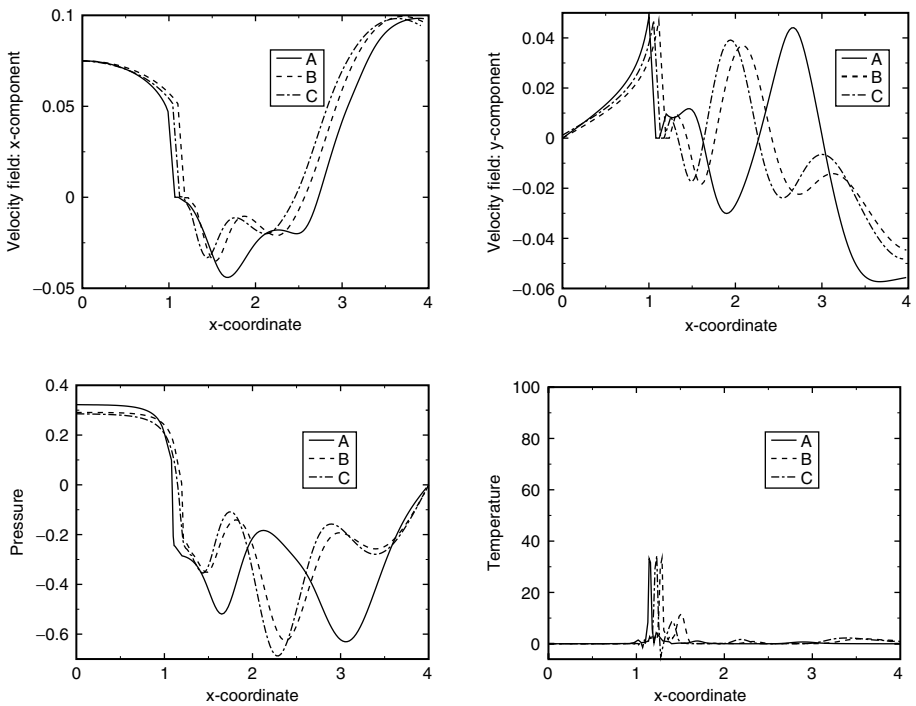

Figure 6. Profiles of the Velocity field x-component (Top Left) and y-component (Top Right), Pressure (Bottom Left) and Temperature (Bottom Right) evaluated along the section $y = 0.5$ for $0 \leq x \leq 4$ at the time $t = 5$ for Cases A,B,C.

94000. However Figure 5 on the right shows that the only part of the system, subjected to high vorticity is the region downstream of the beam. In the region upstream of the beam and in the upper part of the domain the velocity field is almost steady.

One of the motivations of this work was to develop efficient algorithms to solve fluid-structure applications involving non-matching grids. In order to obtain more efficient distributed computations, the solution to the associated coupled problem must be evaluated at varying mesh levels. For instance, performing the computations at mesh l_2 or l_1 in parts of the domain where the mesh l_3 is not needed can reduce the degrees of freedom. To evaluate the efficiency of the computations we split the domain Ω into three subdomains Ω^1, Ω^2 and Ω^3 over which three different non-conforming meshes are built, respectively. The subdomains and the three different non-matching grid configurations considered are shown in Figure 7. In the subdomain Ω^3 which is the solid domain Ω_s, the mesh l_1 is always used. Note that this is because the displacement is solved on a fixed grid. In the first configuration, P_1 (top-right), the meshes, l_2 and l_1, are considered for the subregions Ω^2 and Ω^1, respectively. The different couplings of meshes, l_3-l_2 and l_3-l_1 are used in the same subregions for the second configuration P_2 (bottom-left), and the third configuration P_3 (bottom-right). Note that each of these configurations are based on mid-point refinements and are therefore easier to implement and

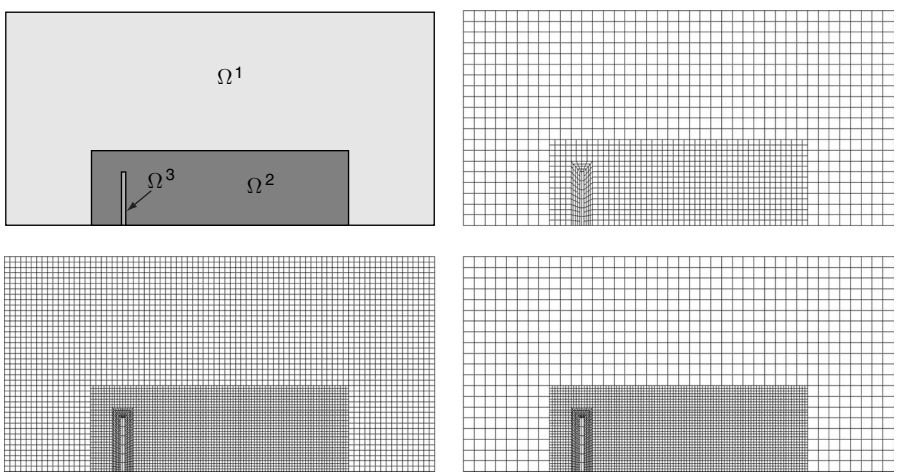

Figure 7. Domain decomposition (top-left) and the different configurations P_1 (top-right), P_2 (bottom-left), P_3 (bottom-right).

test. Further, they also allow for studies involving non-matching grids. The numbers of nodes is greatly reduced for all the three non-conforming configurations. In particular approximatively 11000, 39000 and 28000 are the new numbers of unknowns for the new configurations P_1 P_2 and P_3, respectively. The computational CPU time and the memory allocation expenses are consequently reduced.

In Figure 8, the deflection of the beam extreme point is compared (for the three conforming meshes l_1, l_2 and l_3, and for the 3 non-conforming meshes P_1,

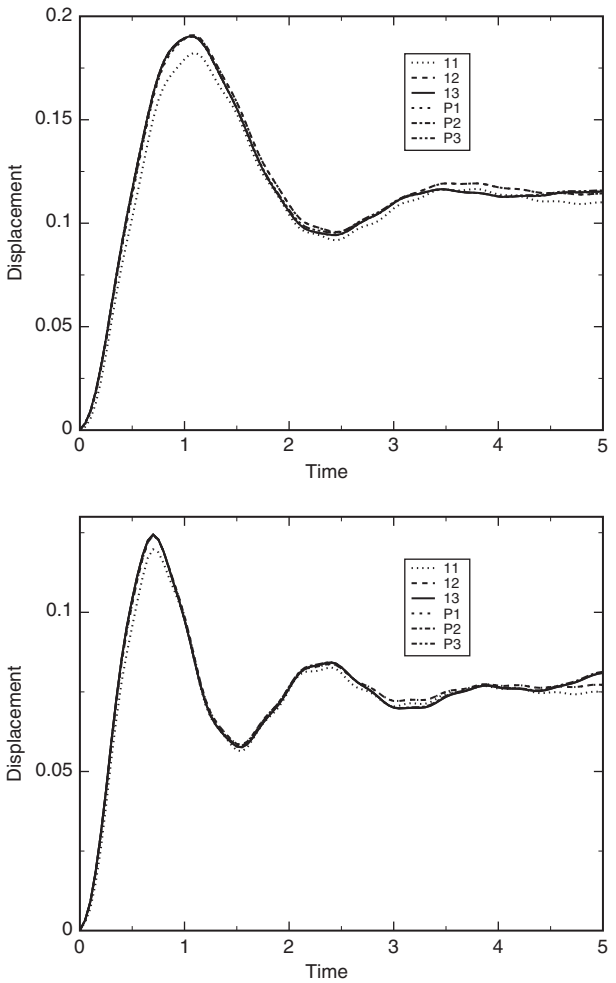

Figure 8. Deflection of the beam extreme point for conforming and nonconforming meshes: Linear (top-panel) and Nonlinear (bottom-panel).

P_2 and P_3) for both the linear (top-panel) and the non-linear (bottom-panel) cases. The results show clear advantages of the non-conforming discretizations over the conforming ones. Obviously the path obtained with the finest mesh l_3 can be considered the most accurate. The l_2 path is very close to the l_3 in the first second but differences appear as soon as the time increases. The l_1 path is always below the l_3, showing too much stiffness in the beam response. The beam oscillation obtained with the non-conforming configuration P_1 perfectly overlaps the result obtained with the conforming mesh l_2, and the result obtained with the configuration P_2 perfectly overlaps the result in l_3. It is possible to find very small differences between the path in l_3 and the path in P_3, where there are two meshs between the two adjacent regions Ω^1 and Ω^2. These results clearly indicate how one can use the non-conforming multilevel partitioning to preserve the same accuracy in regions of interest, reducing at the same time the degree of freedom in other parts of the domain. It must also be pointed out that the nonlinear beam case (bottom-panel) yields a deflection that is much stiffer than the linear beam case (top-panel). This suggests the importance of the influence of the coupling between the axial and transverse beam deflection to the overall coupled system.

6. DISCUSSION AND CONCLUSIONS

This paper presents a distributed computational methodology for solving Fluid-Structure-Thermal interaction problems. A benchmark application that models the interaction of a nonlinear beam structure in a fluid medium along with temperature equations has been studied and tested. Our computational results indicate that the methodology described in conjunction with the multilevel multigrid method leads to a flexible algorithm that can be used to solve coupled FSTI problems over non-matching grids.

We hope to test the performance of the computational methodology presented in a parallel environment for fluid-structure applications with non-matching grids. More specifically, we plan to perform load balancing, scalability studies and analyze the results of the CPU times and speed-ups obtained in a parallel infrastructure. We also plan to perform a detailed hp-version analysis of the methodology presented in this paper. These will be the focus of a forthcoming paper.

REFERENCES

1. Bathe, M. and Kamm, R.D., A Fluid-Structure Interaction Finite Element Analysis of Pulsatile Blood Flow Through a Compliant Stenotic Artery, *Journal of Biomechanical Engineering*, 1999, 121, 361–369.

2. Nobile, F., *Numerical approximation of fluid-structure interaction problems with application to haemodynamics*, Ph.D. Thesis, EPFL, Lausanne, 2001.
3. Ferguson, L., *A computational model for flexible wing based micro air vehicles*, Masters Thesis, Texas Tech University, 2006.
4. Bernardi, C., Maday, Y. and Patera, A., Domain decomposition by the mortar element method, *Asymptotic and numerical methods for partial differential equation with critical parameters. H.K. et al. eds, Reidel, Dordecht*, 1993, 269–286.
5. Ben Belgacem, F., The mortar finite element method with Lagrange Multipliers, *Numererishe Mathematik*, 1999, 84(2), 173–197.
6. Seshaiyer, P. and Suri, M., *hp* submeshing via non-conforming finite element methods, *Computer Methods in Applied Mechanics and Engineering*, 2000, 189, 1011–1030.
7. Ben Belgacem, F., Chilton, L.K. and Seshaiyer, P., The *hp*-Mortar Finite Element Method for Mixed elasticity and Stokes Problems, *Computers and Mathematics with Applications*, 2003, 46, 35–55.
8. Casadei, F., Fotia, G., Gabellini, E., Maggio, F. and Quarteroni, A., A mortar spectral/finite element method for complex 2D and 3D elastodynamic problems, *Computer Methods in Applied Mechanics and Engineering*, 2002, 191, 5119–5148.
9. Aulisa, E., Manservisi, S. and Seshaiyer, P., A computational multilevel approach for solving 2D Navier-Stokes equations over non-matching grids, *Computer Methods in Applied Mechanics and Engineering*, 2006, 195, 4604–4616.
10. Aulisa, E., Manservisi, S. and Seshaiyer, P., A non-conforming computational methodology for modeling coupled problems, Nonlinear Analysis, 2005, 6, 1445–1454.
11. Aulisa, E., Manservisi, S. and Seshaiyer, P., A multilevel domain decomposition approach to solving coupled applications in computational fluid dynamics, International Journal for Numerical Methods in Fluids, 2008, 56, 1139–1145.
12. Braess, D., Dahmen, W. and Wieners, C., A Multigrid Algorithm for the Mortar Finite Element Method, *SIAM Journal of Numerical Analysis*, 1999, 37(1), 48–69.
13. Gopalakrishnan, J. and Pasciak, J.E., Multigrid for the Mortar Finite Element Method, *SIAM Journal of Numerical Analysis*, 2000, 37(3), 1029–1052.
14. Reddy, J.N., *An Introduction to Nonlinear Finite Element Analysis*, Oxford University Press, Oxford, 2004.
15. Girault, V. and Raviart, P., *The Finite Element Method for Navier-Stokes Equations: Theory and Algorithms*, Springer, New York, 1986.
16. Temam, R., *Navier-Stokes equation*, North-Holland, Amsterdam, 1979.
17. Swim, E.W. and Seshaiyer, P., A nonconforming finite element method for fluid-structure interaction problems, *Computer Methods in Applied Mechanics and Engineering*, 2006, 195(17–18), 2088–2099.

18. Donea, J., Giuliani, S., Halleux, J., An arbitrary Lagrangian Eulerian finite element method for transient fluid-structure interactions, *Computer Methods in Applied Mechanics and Engineering*, 1982, 33, 689–723.
19. Grandmont, C., Guimet, V., Maday, Y., Numerical analysis of some decoupling techniques for the approximation of the unsteady fluid structure interaction, *Mathematical Models and Methods in Applied Sciences*, 2001, 11, 1349–1377.
20. Hughes, T., Liu, W., Zimmermann, T., Lagrangian Eulerian finite element formulation for incompressible viscous flows, *Computer Methods in Applied Mechanics and Engineering*, 1981, 29, 329–349.
21. Schafer, M. and Turek, S., *The benchmark problem: flow around a cylinder, in Flow simulation with high performance computers II. (E.H. Hirschel ed.)*, Notes on Numerical Fluid Mechanics, 1996, 52, 547.
22. Turek, S., Efficient solvers for incompressible flow problems: an algorithmic and computational approach, *Lecture Notes in computational science and engineering*, 1999, 6, Springer.
23. Vanka, S., Block-implicit multigrid calculation of two-dimensional recirculation flows, *Computer Methods in Applied Mechanics and Engineering*, 1986, 59(1), 29–48.